The Deep SWIRE Field

III. WIYN Spectroscopy

Frazer N. Owen,[1,2], & G. E. Morrison,[2,3,4]

ABSTRACT

We present the results of spectroscopy using HYDRA on the WIYN 3.5m telescope of objects in the deep SWIRE radio field. The goal of the project was to determine spectroscopic redshifts for as many of the brighter objects in the field as possible, especially those detected in the radio and at 24μm. These redshifts are primarily being used in studies of galaxy evolution and the connection of that evolution to AGN and star-formation. Redshifts measured for 365 individual objects are reported. The redshifts range from 0.03 to 2.5, mostly with $z < 0.9$. The sources were selected to be within the WIYN HYDRA field of approximately 30′ in radius from the center of the SWIRE deep field, $10^h46^m00^s$, 59°01′00″ (J2000). Optical sources for spectroscopic observation were selected from a r-band image of the field. A priority list of spectroscopic targets was established in the following order: 20cm detections, 24m detections, galaxies with $r < 20$ and the balance made up of fainter galaxies in the field. We provide a table listing the galaxy positions, measured redshift and error, and note any emission lines that were visible in the spectrum. In practice almost all the galaxies with $r < 19$ were observed including all of the radio sources and most of the 24μm sources with $r < 20$ and a sample of radio sources which had fainter optical counterparts on the r-band image.

Subject headings: cosmology: observations — galaxies: evolution — galaxies: starburst — infrared: galaxies galaxies

---

[1]National Radio Astronomy Observatory, P. O. Box O, Socorro, NM 87801 USA.; fowen@nrao.edu The National Radio Astronomy Observatory is facility of the National Science Foundation operated under cooperative agreement by Associated Universities Inc.

[2]Visiting astronomer, Kitt Peak National Observatory, National Optical Astronomy Observatories, operated by AURA, Inc., under cooperative agreement with the National Science Foundation.

[3]Institute for Astronomy, University of Hawaii, Honolulu, 96822, USA

[4]Canada-France-Hawaii Telescope, Kamuela, Hawaii, 96743,USA

1. Introduction

This paper is the third in a series documenting our study of the deep SWIRE field centered at $10^h46^m00^s$, $59°01'00''$(J2000). Paper I (Owen & Morrison 2008) describes the 20cm VLA observations which produced the deepest 20cm radio survey to date with 2050 sources and the basic radio properties of the faint μJy population. Paper II (Owen et al. 2009) details a complementary, deep 90cm survey and dependence of 20cm to 90cm spectral index on radio flux density. These two papers concentrate only on radio properties. What is needed to learn more are the distances to the sources and their properties at other wavelengths. In paper IV (Strazzullo et al. 2009) we discuss the absolute radio/optical/NIR properties of the radio sources and their connection to the evolution of galaxies. We accomplish this goal by estimating photometric redshifts for the sources for which we do not possess a spectroscopic redshift, using images of the field from the GALEX uv bands, ground-based UgrizJHK and the 3.6 and 4.5 μm bands of IRAC on Spitzer. As part of our photometric technique we need spectroscopic redshifts as a training set. The results described in this paper are used in paper IV, along with redshifts from other projects for this purpose. These spectroscopic redshifts also provide secure, accurate redshifts, and thus distances, for a large fraction of the low redshift objects in the field.

The results reported here have already been used as calibration data for another photometric redshift study (Rowan-Robinson et al 2008), which has itself been used for in a number of subsequent studies. A secondary goal of the survey was to observe 24μm sources and those redshifts were used for a determination of the 24μm luminosity function (Onyett et al. 2006). Moreover these spectroscopic and the photometric redshifts from paper IV are being used for a number of studies of the AGN versus star-formation activity versus redshift. In addition, deep Spitzer MIPS imaging is being stacked as a function of radio luminosity and redshift in order to use the radio-FIR relation to indicate the relative evolution of these two properties. The redshifts are also being used with the Chandra survey of this region to study the evolution of the X-ray-loud AGN population and its connection to the radio population (Wilkes et al. 2009). Several other studies that are currently underway are also making use of the WIYN redshifts and the photometric redshifts in order to fold the deep radio data into a more complete picture of galaxy evolution provided at other wavelengths.

2. Selection, Observations and Reduction

The sources were selected to be within the WIYN HYDRA field of view, approximately $30'$ in radius from the center of the SWIRE deep field, $10^h46^m00^s$, $59°01'00''$ (J2000). Optical sources for observation were selected the r-band image of the field taken for the SWIRE survey with the KPNO 4m (Lonsdale et al. 2003). The magnitudes were measured using a $2''$ diameter aperture, which is the same size as the fibers. A preliminary 20cm radio image from the VLA and a preliminary 24μm from Spitzer existed at the time of the observation. A priority list of possible sources was established: 20cm detections , 24μm detections, galaxies with $r < 20$, and fainter galaxies ($r > 20$) in the field. As described below sources for observations were optimized for each fiber set.

The observations were made Feb 11-15, 2004 using the HYDRA fiber spectrograph on the WIYN 3.5m telescope at KPNO. The 316@7.0 grating was used with the Bench Spectrograph and the red fiber cables. The G4 $GG - 420$ blocking filter was used which after calibration yielded a usable spectral region of 4400Å to 9700Å with some second order contamination beyond 8800Å. Two CuAr comparison lamp exposures were taken for each wavelength calibration, one with $10\times$ the integration time of the other, were observed before and after each fiber set. These data showed that the wavelength response of the bench spectrograph setup was very stable. Standard stars were observed each night though single fibers to allow a rough relative spectral calibration to be obtained. Radial velocity standards were also observed to check the stability and accuracy of the redshift measurements. These observation demonstrated that the overall calibration of our unknown sources were limited by other considerations than the calibration, mainly S/N.

The fiber setup was done using *whydra*. A large number of runs of the program with slightly different parameters were used to obtain the best fiber setup for each observation. Typically, 20 sky fibers, 5 FOPS (guide stars) and 65 objects fibers were used. Depending on observing conditions different criteria were used to prioritize the setup, *e.g.* brighter objects were observed preferentially when the transparency and/or seeing was poorer. Total observing times of one to four hours were used, usually split into four shorter exposures in order to allow easier removal of cosmic rays. We observed 12 separate, useful fiber configurations with nearly the same pointing center but slightly shifted to reduce the number of the fiber collisions which limited the number of sources we could observe at once. The weather and other conditions, clouds, seeing, position of the moon, varied as usual over the run and we worked our way through our priority list. We were able to examine the spectra in real time and evaluate how well we were doing. We used this information as we went along to plan the next fiber configuration. For example if the transparency and/or seeing were likely to be poor during a fiber set we picked brighter, sometimes low priority objects, to observe. At times we observed a brighter set of objects with a shorter total observing time in order to have all the observations of a given fiber set fit into the time during a single night. In the end, these constraints made the data quality of the spectra somewhat variable and at times we lost high priority objects entirely.

The IRAF *ccdproc* package was used for the reductions. First the observations were bias corrected and then the *dohydra* script was used. Dome flats were used both to determine the locations of the fibers on the CCD and for flat fielding. The two comparison lamp exposures were combine so that good S/N could be obtained in both the red and blue parts of the spectrum. Bad sky frames were edited out during the procedure. The individual spectra were extracted to a one-dimensional format and then combined using the IRAF task, *scombine*. The final spectra were then edited using *splot*. Redshifts were derived either by calculating equivalent widths and center wavelengths for individual lines, mostly emission lines, in each spectrum using *splot* or cross-correlating absorption-line spectra with standard spectra using the IRAF task *fxcor*. Either a radial velocity standard or elliptical galaxies obtained in previous observing runs with wider spectral coverage and better spectral resolution were used as the template spectrum. Errors were estimated by combining the internal errors from the cross-correlations for absorption spectra, or the scatter in the redshift estimates for multiple lines in quadrature with 50 km s^{-1}, the upper limit to the error in the absolute spectral calibration derived from the scatter in velocity derived for observations of radial velocity standard stars.

In figure 1, we show six examples of spectra we used in to determine the results in tables. These spectra are picked to cover the range of different types of objects in our sample from broad-line, high redshift AGN to pure absorption-line spectra. One can see the increasing importance of night sky features at longer wavelengths but that strong emission lines can still be seen in the red. After completing the reductions out of 1063 objects in our original sample, 548 had a least one reduced spectrum. Of these we obtain reliable redshifts for 365 objects. For the remaining 183 we could not measure a robust redshift. In most of these cases the signal in the spectrum was too weak to be usable due to poor observing conditions. In table 1 we summarize the statistics of the observed sources as a function of r magnitude.

3. Results

In table 2, we give the first ten columns of the electronic table containing J2000 positions and r magnitudes of the objects with for which we obtained successful spectra from WIYN. In table 3, we present the first ten columns of the electronic table containing the results of the WIYN spectroscopy. In columns 1 and 2, we give the J2000 coordinate name and the radio source name. If column 2 is blank that means that the galaxy was not detected in the five sigma 20cm catalog given in paper I. Columns 3 and 4 contain the redshift and error. In column 5 we give the “notes” on the results, including either the spectral line(s) and/or the “FXCOR” if the redshift was obtained by cross-correlation with an absorption-line template.

When a photometric redshift is used to confirm a one line redshift we add the note “photoz’. If the source was detected at 20cm at the three sigma or four sigma level we also note that in column 5. Finally, we give the number of the galaxy in the input file for the WIYN observation for future reference and requests for individual spectra.

Of the 365 total objects for which we measured a redshift, 267 of the objects have emission lines; 249 have two or more lines. For the 18 objects with only one line, the identity of the emission line (usually OII) is confirmed by an absorption line redshift in nine cases and in the other nine cases by a photometric redshift from Strazzullo et al. (2009). 98 objects have measured redshifts from absorption lines only. 249 of the measured redshifts are for radio detected objects. 229 are published in the five sigma catalog in paper I. Ten are detected at the four sigma level and ten more at three sigma. 286 24mμ sources had their redshifts determined (Onyett et al. 2006). In Figure 2 we show the redshift distribution. The largest peak contains 53 objects with $0.11 < z \leq 0.12$ suggesting we are looking through an organized structure at this redshift, although no concentrated cluster is obvious in the images. Eight objects not shown have redshifts > 1.

REFERENCES

Lonsdale, C. J. and 36 Co-authors 2003 PASP, 115, 897.

Onyett, N., Oliver, S., Morrison, G., Owen, F., Pozzi, F., Carson, D. & the SWIRE team in "The Spitzer Space Telescope: New Views of the Cosmos" edited Armus, L. and Reach, W. T. 2006, ASP Conference Series, 357, 275.

Owen, F. N. & Morrison, G. E. 2008 AJ, 136, 1889 (paper I).

Owen, F. N., Morrison, G. E., Klimek, M., & Greisen, E. C. 2009 (submitted) (paper II).

Rowan-Robinson, M. & 18 other authors 2008 MNRAS, 386, 697.

Strazzullo, V. et al. 2009 (in preparation).

Wilkes, B. J., Kilgard, R., Kim, D-W., Kim, M., Polletta, M., Lonsdale, C., Smith, H. E., Surace, J., Owen, F. N., Franceschini, A., Siana, B. & Shupe, D. 2009, submitted.

Table 1. Observed Source Statistics

r Mag	# in cat	# observ	# z meas
$r \leq 19$	73	72	67
$19 < r \leq 20$	218	176	129
$20 < r \leq 21$	633	189	125
$21 < r \leq 24$	139	111	44
all	1063	548	365

Table 2. Observed Source Positions

Name	RA(2000.0)	Dec(2000.0)	r Mag
104340+591241	10 43 40.32	59 12 41.1	19.3
104340+591826	10 43 40.77	59 18 26.4	19.0
104341+591733	10 43 41.38	59 17 33.7	19.9
104341+591654	10 43 41.50	59 16 54.0	18.3
104342+591158	10 43 42.22	59 11 58.2	19.4
104343+585535	10 43 43.21	58 55 35.7	19.9
104347+584756	10 43 47.17	58 47 56.9	20.1
104347+590217	10 43 47.61	59 02 17.3	19.5
104347+590620	10 43 47.81	59 06 20.9	19.3
104351+585544	10 43 51.24	58 55 44.2	21.0

Table 3. Redshifts and Associated Data

Coord Name	Radio Name	z	error z	Notes
104340+591241		0.1994	0.0002	OIII, NII, Ha, Hb, 4sigma 7077
104340+591826		0.0281	0.0002	NII, SII, Ha 7043
104341+591733		0.2286	0.0002	OIII, NII, Ha, Hb 7186
104341+591654		0.0286	0.0002	OIII, OI, NII, SII, HeI, Ha, Hb 7016
104342+591158		0.1994	0.0002	FXCOR 7087
104343+585535		0.4714	0.0002	OII, OIII, Hb, Hg, Ha, NII Balmer lines broad 7183
104347+584756		0.4187	0.0003	FXCOR 7250
104347+590217		0.3223	0.0003	FXCOR 7101
104347+590620	10061	0.1417	0.0002	OIII, OI, NII, SII, HeI, Ha, Hb 4sigma 7076
104351+585544	00053	0.6038	0.0003	OII, OIII, Hb 7741

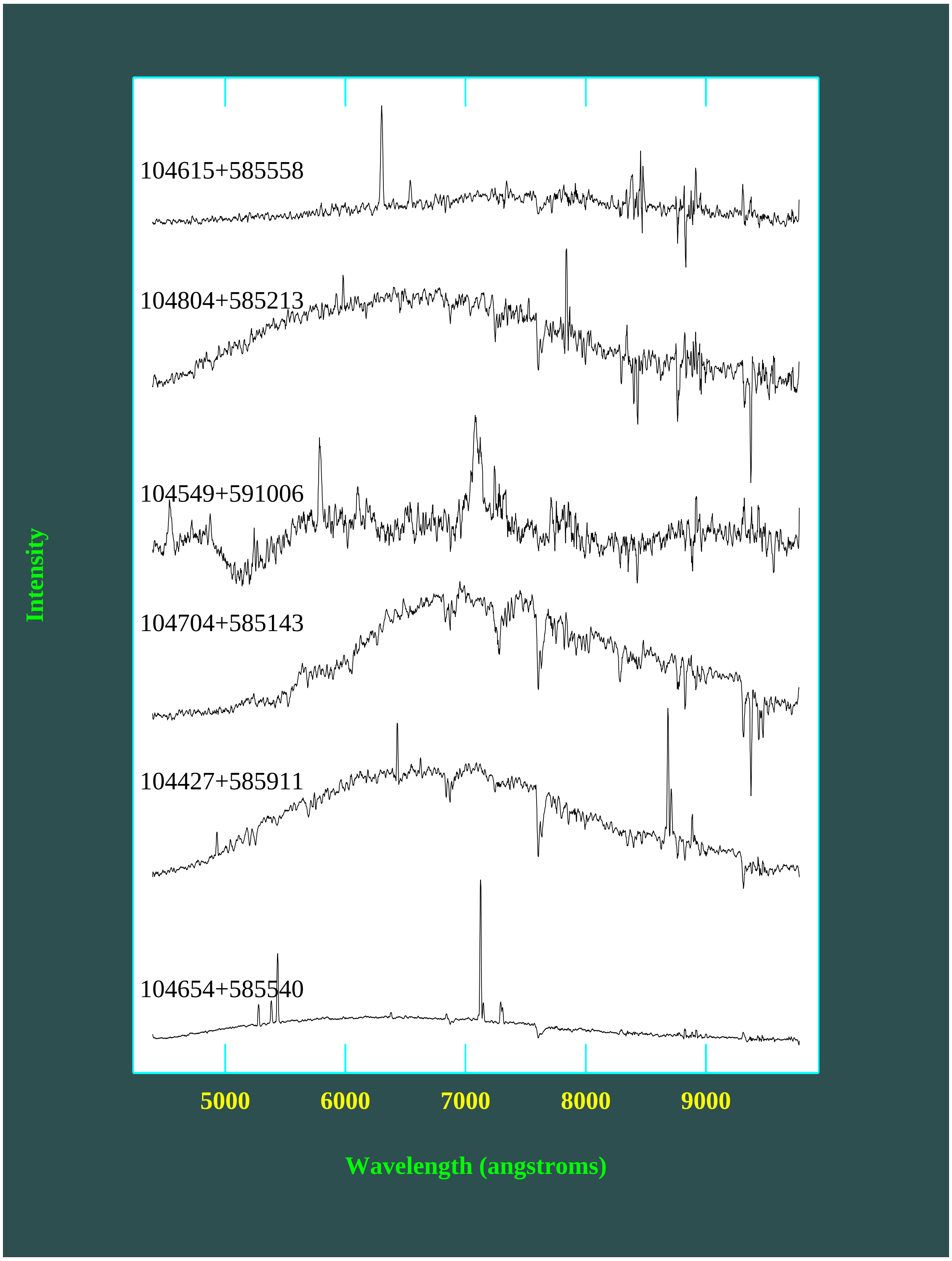

Fig. 1.— Examples of the observed, uncalibrated spectra used to estimate redshifts. 104615+585558: $z = 0.68$, narrow emission lines; 104804 + 585213: $z = 0.19$, weak emission lines; 104549 + 591006: $z = 2.75$, broad emission lines; 104704 + 585143: $z = 0.41$, old stellar population absorption lines; 104427 + 585911: $z = 0.32$, narrow emission lines; 104654 + 585540: $z = 0.12$, strong emission lines. See table 3 for details of lines used for redshifts.

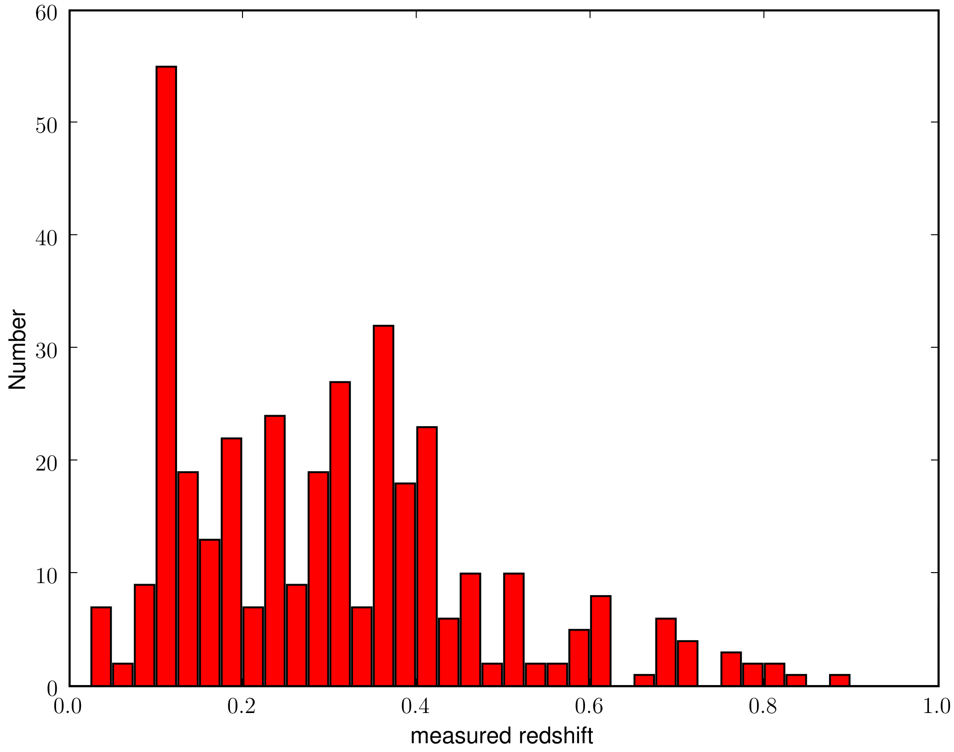

Fig. 2.— Histogram of redshift distribution $0.0 < z < 1.0$. Eight objects have measured redshifts in the range $1.0 < z < 2.75$.